

available evidence indicates that protons cannot directly produce such effects. Rather, large fluxes of slow protons have been thought to be capable of producing only a "haze or graying of the visual field" (3). Such an effect, "like snow on a TV screen," was reported in addition to the distinct flashes in the SAA during the second session, but the PLT could not distinguish this phenomenon from normal background visual phosphenes or "noise." He did remark, however, that this "noise" was gone and that he was seeing "just darkness" immediately after exiting the SAA. If the protons do not cause the flashes directly, then we are left with two immediate alternatives. Either the flashes were caused by heavier ( $Z \geq 2$ ) secondaries from proton interactions in the surrounding matter, or they were caused by an as yet unobserved heavy ( $Z \geq 2$ ) component of the inner belt trapped radiation, whose flux one would a priori expect to be approximately proportional to that of the trapped protons.

To explore these two possibilities further, a very detailed Monte Carlo program was devised to examine the charged particle flux in the vicinity of the retina (9). This program included the specific geometric properties of the actual incident charged particle flux, the spacecraft shielding, and the head and eyes of the crewman for each of the cases simulated. The incident particles were propagated with allowance for both energy loss and spallation. Three physiological parameters were used to determine if a particle would produce a flash. These are: (i) a minimum required linear energy transfer (threshold LET) of the particle in the sensitive region of the retina, (ii) a minimum required length of the track in the sensitive region projected onto a plane tangent to the surface of the retina, and (iii) the thickness of the sensitive retinal region which can respond to this stimulus. No attempt was made to include observer efficiencies. It was assumed that a 100 percent flash-producing efficiency existed for particles above the threshold determined by the three parameters and 0 percent for those below that threshold. In order to best fit the Skylab non-SAA data from both sessions and all of the Apollo light flash data with the same physiological parameters, the calculation shows, for example, that for a threshold LET of  $\sim 37 \text{ keV}/\mu\text{m}$  (which is consistent with heavy ion accelerator light flash experience), a sensitive layer thickness of the retina of  $50 \mu\text{m}$  and a minimum projected path length of  $40 \mu\text{m}$  result. Since the parameters are coupled to each other, a range of reasonable values of the parameters was explored. The results

for the various non-SAA flux environments have been indicated in Fig. 2. Finally, when an all-proton SAA flux equal to the maximum intensity known to exist at Skylab altitudes is employed with the Skylab non-SAA/Apollo parameter values in an attempt to simulate the SAA observations during the second session, the secondary alpha ( $I_0$ ) flux fails to produce the maximum observed flash rate by a factor of 5 to 10 (11). A further calculation was carried out to determine the flux of multiply charged trapped particles required to produce the observed flash rate. This proved to be about one effective particle per 6000 trapped protons, a number consistent with the upper limits currently available from direct measurements.

We do not claim to have demonstrated the existence of trapped  $Z \geq 2$  particles in the inner radiation belts. Rather we suggest that, on the basis of these light flash observations, it is one possible solution.

L. S. PINSKY  
W. Z. OSBORNE

*Physics Department, University of Houston, Houston, Texas 77004, and National Aeronautics and Space Administration, Johnson Space Center, Houston 77058*

R. A. HOFFMAN, J. V. BAILEY  
*National Aeronautics and Space Administration, Johnson Space Center*

## References and Notes

1. For a discussion of the radiation belts and the SAA see, for example, W. N. Hess, *The Radiation Belt and the Magnetosphere* (Blaisdell, Waltham, Mass., 1968).
2. G. G. Fazio, J. V. Jelley, W. N. Charman, *Nature (Lond.)* **228**, 260 (1971); R. Madey and P. J. McNulty, in *Proceedings of the National Symposium on Natural and Man-Made Radiation in Space*, E. A. Warman, Ed. (NASA Publication TM X-2440, National Aeronautics and Space Administration, Washington, D.C., 1972), pp. 757 and 767; J. R. McAulay, *Nature (Lond.)* **232**, 241 (1971).
3. T. F. Budinger, H. Bichsel, C. A. Tobias, *Science* **172**, 868 (1971).
4. H. H. Heckman and A. H. Armstrong, *J. Geophys. Res.* **67**, 1255 (1962).
5. R. A. English, R. E. Benson, J. V. Bailey, C. M. Barnes, *Apollo Experience Report—Protection against Radiation* (NASA Publication TN D7080, National Aeronautics and Space Administration, Johnson Space Center, Houston, Tex., 1973), pp. 3–5.
6. B. L. Cash, Report No. EPS-956 (Lockheed Electronics Company, Houston, Tex., 1972).
7. L. S. Pinsky, W. Z. Osborne, J. V. Bailey, R. E. Benson, L. F. Thompson, *Science* **183**, 957 (1974).
8. For example, see L. G. Parratt, *Probability and Experimental Errors in Science* (Wiley, New York, 1961), p. 140.
9. A detailed article describing the Monte Carlo calculations will be published elsewhere (W. Z. Osborne and L. S. Pinsky, in preparation).
10. Measured secondary production cross sections were used, and all approximations were conservative to produce a maximum secondary flash rate.
11. The maximum flash rate one would expect from secondary alphas is  $\leq 3$  flashes per minute, whereas the maximum observed rate is  $> 20$  flashes per minute.
12. We thank all of the flight controllers, flight planners, and support personnel at the Johnson Space Center who aided us during the experiment, and the Skylab flight crews whose competence and cooperation in this effort were outstanding.

7 October 1974; revised 27 January 1975

## Binary Pulsar PSR 1913 + 16: Model for Its Origin

**Abstract.** *The existing observational data for the binary pulsar PSR 1913 + 16 are sufficient to give a rather well-defined model for the system. On the basis of evolutionary considerations, the pulsar must be a neutron star near the upper mass limit of 1.2 solar masses ( $M_{\odot}$ ). The orbital inclination is probably high,  $i \gtrsim 70^{\circ}$ , and the mass of the unseen companion probably lies close to the upper limit of the range  $0.25 M_{\odot}$  to  $1.0 M_{\odot}$ . The secondary cannot be a main sequence star and is probably a degenerate helium dwarf. At the 5.6-kiloparsec distance indicated by the dispersion measure, the magnetic dipole model gives an age of  $\sim 4 \times 10^4$  years, a rate of change of the pulsar period of  $\dot{P} \sim 2$  nanoseconds per day, and a surface magnetic field strength  $\sim 1/10$  that of the Crab pulsar. The pulsar is fainter than an apparent magnitude  $V \sim +26.5$  and is at least  $\sim 80$  times fainter than the Crab pulsar in the x-ray band. The companion star should be fainter than  $V \sim +30$ , and a radio supernova remnant may be detectable near the position of the pulsar at a flux level of  $\leq 10$  janskys. Important tests of this model will be provided by more accurate measurement of  $\dot{P}$  and by a careful search for a faint supernova remnant.*

Taylor and Hulse (1) have recently reported the detection of a new pulsar, with period  $P \approx 59$  msec, at the position: right ascension  $\alpha_{1950} = 19^{\text{h}}13^{\text{m}}13^{\text{s}} \pm 4$  seconds, declination  $\delta_{1950} = +16^{\circ}00'24'' \pm 60''$ . The dispersion measure is  $167 \pm 5 \text{ cm}^{-3}$  parsec, implying a distance of  $\sim 5.6$  kiloparsecs, for an electron density of  $0.03 \text{ cm}^{-3}$ . The source is correspondingly weak, with an average flux density of  $0.006$  jansky ( $1 \text{ Jy} = 10^{-26} \text{ watt m}^{-2} \text{ hertz}^{-1}$ ).

This remarkable object is the first pulsar to show reliable evidence of binary motion. The orbital parameters (1) are as follows: orbital period  $P_{\text{orb}} = 27,908 \pm 7$  seconds  $\approx 7.5$  hours; radial velocity semi-amplitude =  $199 \text{ km sec}^{-1}$ ; orbital eccentricity  $e = 0.615$ ; projected semimajor axis of pulsar orbit =  $a_n \sin i = 1.0 R_{\odot}$ , where  $i$  is the orbital inclination and  $R_{\odot}$  is the solar radius; and mass function  $f(m) = 0.13 \pm 0.01 M_{\odot}$ , where  $M_{\odot}$  is the solar

mass. We show here that these data are sufficiently restrictive to lead to a nearly unique model amenable to observational test.

The shortness of the period  $P \equiv 2\pi/\omega \sim 59$  msec ( $\omega$  is the angular frequency of rotation) shows that the new pulsar must be a neutron star. The age can be computed from the magnetic dipole model of Ostriker and Gunn (2). Gravitational radiation losses are negligible ( $\sim 5$  percent); thus the age of the pulsar is  $1/2 \tau_m$ , where

$$\tau_m \equiv \frac{3c^3 I}{2m_{\perp}^2 \omega^2} \quad (1)$$

Here  $c$  is the speed of light,  $m_{\perp} \sim BR_n^3$  is the perpendicular component of the magnetic dipole moment,  $I \sim M_n R_n^2 \sim 10^{45}$  g cm<sup>2</sup> is the moment of inertia,  $B$  is the surface magnetic field strength, and  $M_n$  and  $R_n$  are the mass and radius, respectively, of the neutron star. The quantity  $I$  is not a strong function of  $M_n$ , and, therefore, if the magnetic moments are comparable, the ages of the pulsars are inversely proportional to  $\omega^2$ . The observed rates of period change for the Crab pulsar, NP 0532, and the Vela pulsar, PSR 0833, can be scaled to the rotation frequency  $P \approx 59$  msec to yield an estimate of the age of the new pulsar of  $\sim 4 \times 10^3$  years. The measured flux density provides a rough consistency check of this age. The fluxes should be proportional to the magnetic luminosity  $\propto (m_{\perp}^2 \omega^4)$  and inversely pro-

portional to the square of the distance,  $d$ . With allowance for different measurement frequencies, the observed flux of 0.006 Jy at 430 Mhz is significantly smaller than the  $\sim 0.08$  Jy estimated from the Crab [ $\sim 0.2$  Jy at 196 Mhz, for  $d \approx 2$  kiloparsecs (3)] and Vela [ $\sim 0.2$  Jy at 408 Mhz, for  $d \approx 0.5$  kiloparsec (4)]. This implies either that (i) the true distance is as large as 17 kiloparsecs (which we regard as unlikely) or that (ii) the dipole moment of the new pulsar is  $1/3$  that of the Crab or Vela pulsars, and the age is as great as  $4 \times 10^4$  years. Measurement of  $\dot{P}$ , the rate of change of the pulsar period, which we estimate to lie between 2 and 20 nsec day<sup>-1</sup>, would solve this uncertainty in age and distance.

From the observed period and estimated values of  $I$  and  $\tau_m$ , the total luminosity is

$$L = I\omega\dot{\omega} = I\omega^2/\tau_m \sim 5 \times 10^{36} \text{ to } 5 \times 10^{37} \text{ erg sec}^{-1} \quad (2)$$

This is much too high a luminosity to be carried by the radio emission alone, so that the new pulsar must also radiate in the optical and soft x-ray bands. Unfortunately, it is probably undetectable in these bands. The apparent magnitude of the Crab pulsar, averaged over a period, is  $V = +18.2$  (5). Allowing for the greater distance and age (4.7 magnitudes), interstellar absorption (3.6 magnitudes), and the weaker magnetic dipole moment (2.5 magnitudes), our most optimistic estimate for PSR 1913 + 16 is  $V \sim +26.5$ .

The pulsed x- and  $\gamma$ -rays from NP 0532 amount to  $\sim 7$  percent of the total radiation from the nebula plus pulsar (6). The total x-ray intensity of the Crab is  $947 \pm 21$  count sec<sup>-1</sup> (7). The contribution due to the pulsar is thus  $\sim 65$  count sec<sup>-1</sup>. Thus the Crab pulsar, placed at 5.6 kiloparsecs and aged to a period of  $\sim 59$  msec, would produce  $\sim 0.8$  count sec<sup>-1</sup>. This is below the level of detectability ( $\sim 3$  count sec<sup>-1</sup>) of the Uhuru x-ray satellite detectors and is consistent with the failure to detect this source in the x-ray band (7, 8).

With  $f(m)$  and  $a_n \sin i$  known from the observations, the mass  $M_2$  of the secondary star and the separation of the two stars can be found as functions of  $i$  and  $M_n$ . The masses of neutron stars  $M_n$  are known (9) to be confined to the range  $0.1 \lesssim M_n/M_{\odot} \lesssim 1.4$ . This constrains the possible values of  $i$  and  $M_2$ . In Fig. 1 we have plotted the function  $M_2 = M_2(M_n, i)$  for this system. The minimum value is  $M_2 \sim 0.25 M_{\odot}$ , which occurs when  $M_n \sim 0.1 M_{\odot}$  and  $i = 90^{\circ}$ .

Tidal stability provides an extremely important constraint on the nature of the secondary star since each assumed  $i$  and  $M_n$  yields a value for the Roche lobe at periastron, which cannot be exceeded by the radius of the secondary. The semimajor axis of the orbit is given by

$$a = \frac{6.9 \times 10^5 (1 + q)}{\sin i} \text{ km} \quad (3)$$

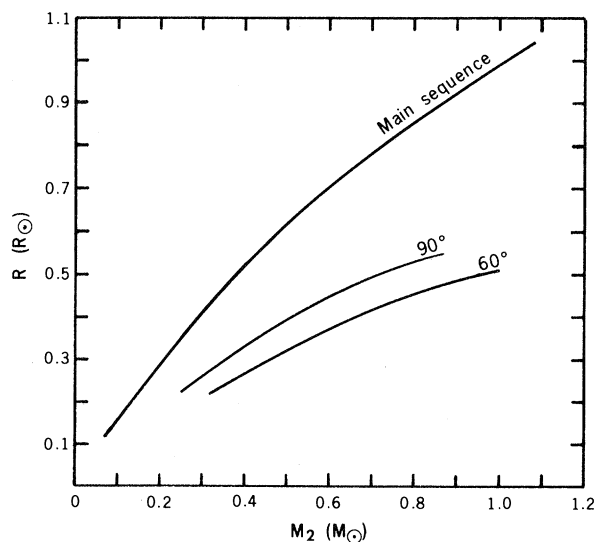
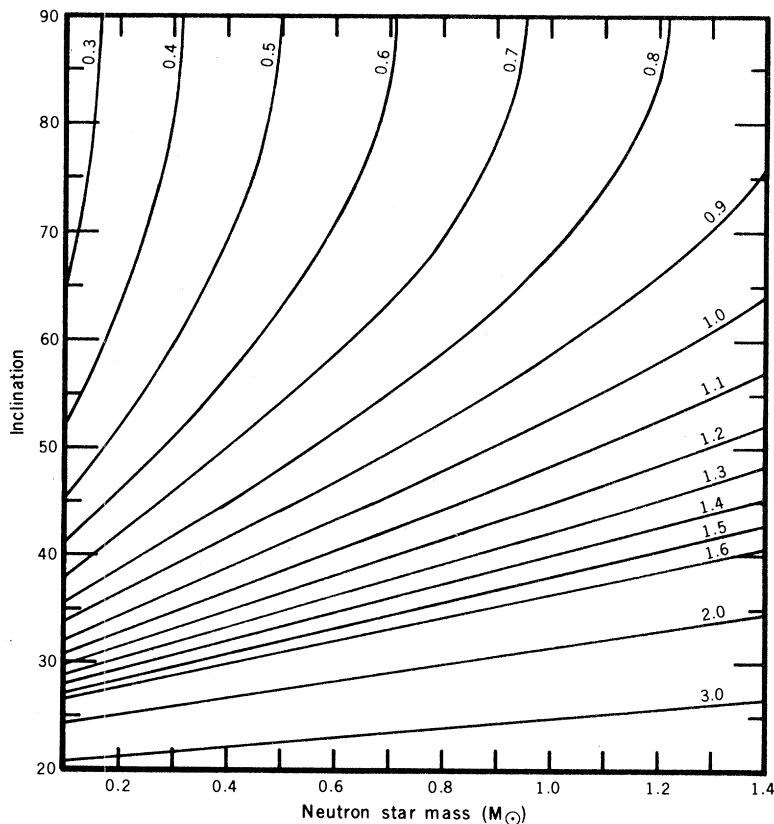


Fig. 1 (left). The mass of the neutron star in PSR 1913 + 16 as a function of the orbital inclination, and the mass of the companion star (shown as the parameter of the different curves in  $M_{\odot}$ ). Fig. 2 (right). The mass-radius relation for hydrogen MS stars [from (11)]. Also shown is the size of the Roche lobe of the companion at periastron for two different inclinations, and for the mass ratio corresponding to  $0.1 M_{\odot} \lesssim M_n \lesssim 1.4 M_{\odot}$ .

where  $q \equiv M_n/M_2$ . For each  $i$  and for  $0.1 \leq M_n/M_\odot \leq 1.4$ , there is a unique  $M_2$  consistent with  $f(m)$ . This gives  $q$ . The separation between the components at periastron is  $a(1-e)$ . Thus we can plot the Roche lobe at periastron (Fig. 2) (10). The results are not very different between  $i = 60^\circ$  and  $i = 90^\circ$ , and  $i \ll 60^\circ$  can be excluded (see below). Also plotted in Fig. 2 is the mass-radius relation for main sequence (MS) stars (11). In all cases the Roche lobe at periastron is smaller than the corresponding MS radius, and the effect becomes more pronounced for smaller values of  $i$ . The secondary star therefore cannot be on the MS but must be a "subluminous star," for example, a hot degenerate star, another neutron star, or a black hole. This is also consistent with the absence of x-ray emission from this system.

It seems unlikely that the secondary star is either a neutron star or a black hole, although neither of these possibilities can yet be excluded. If the rotation axis of the pulsar primary is approximately perpendicular to the orbital plane, a small inclination is difficult to reconcile with the rather narrow emission cone of a pulsar,  $\lesssim 20^\circ$ . This suggests  $i \gtrsim 70^\circ$  and implies  $M_2 \lesssim 1.0 M_\odot$ , from Fig. 1. This does not exclude a low-mass black hole secondary, but stellar evolution in a close binary system probably produces black holes more massive than  $\sim 1.4 M_\odot$ . A second neutron star also appears improbable, since, if we are in the emission cone of either pulsar, we should see both. The present data do not indicate a second pulsar, although this possibility cannot be entirely ruled out (1).

These arguments against the black hole or neutron star nature of the secondary are weak. If they are correct, this star must be an "ordinary subluminous star," such as a shell-burning star, a helium-burning MS star, or a hot degenerate dwarf. Since the pulsar is so young, the companion must be at high luminosity:  $\log L/L_\odot \sim 1.0 \pm 1.0$ . Unfortunately, the large distance, high absorption, and high effective temperature (and thus very large bolometric corrections) make it unlikely that the secondary can be observed optically: we estimate  $V \gtrsim 30$ .

The birth of a neutron star probably occurs in a supernova explosion. Our estimates of the age of the new pulsar place its birth  $\sim 4 \times 10^4$  years ago. This is young enough so that the supernova remnant (SNR) might still be visible optically and should certainly be detectable in the radio band. We have accordingly examined the most recent catalogs of radio and optical SNR's in an effort to find the SNR associated with this pulsar.

Of the 20 known optical SNR's (12) and the  $\sim 100$  known radio SNR's (13), the closest to the position of the new pulsar are 3C 400.2 and CTB 63. Both of these objects, however, are more than  $5^\circ$  away, and at the 5.6-kiloparsec distance and the  $\sim 4 \times 10^4$  year age of PSR 1913 + 16, this implies relative velocities of  $\sim 15,000$  km sec $^{-1}$ . This is so much larger than the orbital velocity of the system ( $\sim 200$  km sec $^{-1}$ ) that it seems very unlikely that either of these SNR's is associated with the pulsar. Consequently the SNR related to this pulsar must have been missed in these surveys either because it was too small or because it was too weak.

The limits of detectability for the two radio SNR catalogs used are fluxes of  $\gtrsim 10$  Jy and an angular size of  $\sim 2'$ . The Crab nebula, which is younger by a factor of  $\sim 40$  and was produced by a relatively weak supernova, has already expanded to a diameter of  $\sim 5'$ . At a distance of 5.6 kiloparsecs, instead of the 2-kiloparsec distance to the Crab, this corresponds to a diameter already  $\sim 2'$ . We therefore regard it as highly unlikely that the SNR which must have been produced coincidentally with the birth of PSR 1913 + 16 is too small to have been included in the radio SNR catalog.

In order to determine whether the SNR is too faint, we note that, if it were still being fed with energetic particles, as the Crab nebula is being energized by its pulsar, the greater distance and age would reduce the  $\sim 10^3$  Jy flux level of the Crab at 1 GHz to  $\sim 1.2$  Jy. The associated SNR thus could indeed have been missed. It is therefore important to carry out a new search to a very much lower level of sensitivity in the area surrounding the pulsar.

If the unseen companion of PSR 1913 + 16 is a hot degenerate star, as we have suggested, it seems quite unlikely that this system was formed by the fission of a single massive star. We shall therefore attempt to understand its origin in terms of normal evolutionary processes.

Let us consider a system that initially (phase I) consists of two stars on the MS: star A with initial mass  $M_A^{(I)} \gtrsim 1.0 M_\odot$  and star B with initial mass  $M_B^{(I)} < M_A^{(I)}$ . It is necessary that  $M_A^{(I)}$  exceed  $\sim 1.0 M_\odot$  in order for star A to evolve off the MS in  $\lesssim 10^{10}$  years, and this requires that the initial orbit must have been larger than the present one. Both the small size of the present orbit and the fact that only a small part of the total mass of the system can have been lost in the supernova event (since the system has remained bound) suggest that the initial mass of the system cannot have been very large. For purposes

of illustration, we shall therefore adopt  $M_A^{(I)} = 2 M_\odot$ ,  $M_B^{(I)} = 1 M_\odot$  in numerical examples.

After  $\sim 10$  to 15 percent of  $M_A^{(I)}$  has been burned into helium, star A begins to evolve off the MS. When it has expanded to fill its Roche lobe, it begins to transfer mass onto star B. Mass exchange terminates when most of the unburned envelope of star A has been lost. At this stage (phase II), the masses of the two stars are thus  $M_A^{(II)} \sim 0.1 M_A^{(I)}$  ( $\sim 0.2 M_\odot$ ) and  $M_B^{(II)} \sim M_B^{(I)} + 0.9 M_A^{(I)}$  ( $\sim 2.8 M_\odot$ ). The rate of evolution of star B thus accelerates, but the MS lifetime of the star is still long enough to allow star A to cool off to  $\sim 10^{-2} L_\odot$  and become a low-mass, virtually pure helium white dwarf with a central temperature  $T_c \lesssim 10^7$  K (14).

At the end of its MS phase, star B now in turn expands to fill its Roche lobe and begins to transfer mass back onto star A. At this stage (phase III), the burned-out helium core of star B has grown to  $\sim 0.1 M_B^{(II)}$  ( $\sim 0.3 M_\odot$ ). Because the orbit is small, mass transfer probably occurs while star B is still close enough to the MS so that the expansion rate (and thus the mass transfer rate) is not extreme ( $\sim 10^{-7}$  to  $10^{-9} M_\odot$  year $^{-1}$ ). These rates are typical of those inferred for the cataclysmic variables (15) and suggest a generic resemblance to such systems at this phase of evolution. Adiabatic compression of the hydrogen-rich material being accreted onto the white dwarf now causes re-ignition of the hydrogen-burning shell source (16), which then undergoes a series of shell flashes (17). These are probably not accompanied by significant (if any) mass loss from star A, however (18). The principal consequence of the shell flashes is thus to cause a gradual growth of the massive, degenerate helium core.

It is during this stage of the evolution that the binary orbit probably takes its present form. There are several possible mechanisms that may be responsible for this contraction. For example, the rate of nuclear burning in the shell flashes may be unable to keep pace with the rate at which mass is transferred from star B. In this case, star A may develop a stable hydrogen-burning shell and attempt to assume a red-giant structure also, so that the common equipotential surface is overfilled. The system would then become a red giant with a binary core, and it seems quite probable that the common envelope would exert sufficient drag to contract the relative orbit of the two cores. Even if a common envelope does not develop, however, gravitational radiation from close binaries causes orbital contraction on about the

time scale observed in some close binary systems (19), and tidal dissipation (20) may also cause a white dwarf to spiral into a red giant on a time scale short enough to be important in this phase.

Mass transfer continues at an accelerating rate during this stage (phase IV) of orbital contraction, and the massive, degenerate helium core of star A continues to grow. It is not clear whether neutrino losses in this phase are sufficient to prevent helium ignition. Even if helium ignition does occur, however, it is unlikely that the radius of the helium core will expand enough to fill its Roche lobe, and the core temperature certainly remains much too low for carbon ignition to occur (21).

We are thus led to a situation in which star A is ultimately pushed over the Chandrasekhar limit by continued accretion of the mass transferred back from star B. At this stage (phase V), the masses of the two stars are  $M_A^{(V)} \sim 1.4 M_\odot$ ,  $M_B^{(V)} \sim M_A^{(I)} + M_B^{(I)} - 1.4 M_\odot$  ( $\sim 1.6 M_\odot$ ); star A is a massive, degenerate white dwarf; star B is evolving toward the red-giant phase and has a degenerate helium core of mass  $\sim 0.1 M_B^{(II)}$  ( $\sim 0.3 M_\odot$ ). At this stage, the core of star A undergoes collapse, and the residual nuclear fuel is ignited to power a supernova explosion.

Most of the energy released in a supernova event is carried off by neutrinos and is unavailable for ejecting mass from the star (22). If a few tenths of a solar mass are ejected with velocities  $\sim 10^4$  km sec $^{-1}$ , as is typical of type I supernovas, the energy content of the ejecta is  $\sim 10^{50}$  ergs. If the radius of the star at the time of the supernova explosion of star A is  $\sim 0.5 R_\odot$ , compared to a separation of  $\sim R_\odot$ , then star B subtends a fractional solid angle  $\Delta\Omega/4\pi \sim 0.1$ . The energy absorbed by the envelope of star B from the expanding supernova shell is thus  $\sim 10^{49}$  ergs, and this is sufficient to eject virtually the entire hydrogen envelope of star B, leaving only the residual helium core with a mass of perhaps  $\sim 0.2 M_B^{(II)}$  ( $0.6 M_\odot$ ) in orbit around the pulsar remnant of mass  $\sim 1.2 M_\odot$ . From Fig. 1 we note that this particular set of parameters is just excluded by the orbital kinematics, but qualitatively similar systems (for example, a  $0.7 M_\odot$  companion and a  $0.98 M_\odot$  pulsar or a  $0.8 M_\odot$  companion and a  $1.2 M_\odot$  pulsar) are entirely possible. The observations thus appear to be entirely compatible with this evolutionary scheme.

On the basis of the analysis presented in this report, we conclude that two of the most important observational programs that should be carried out are (i) the measurement of the long-term average  $\dot{P}$  and

(ii) a search for a radio SNR at the position of the pulsar. We are of course aware that both tidal and general relativistic effects will be important in this system, but a discussion of these effects is beyond the scope of the report. It is clear, however, that this system will be a veritable laboratory for both gravitational theories and the study of neutron star structure.

H. M. VAN HORN  
S. SOFIA\*, M. P. SAVEDOFF  
J. G. DUTHIE  
R. A. BERG

Department of Physics and Astronomy  
and C. E. Kenneth Mees Observatory,  
University of Rochester,  
Rochester, New York 14627

#### References and Notes

1. J. H. Taylor and R. A. Hulse, *Int. Astron. Union Circ. 2704* (4 Oct. 1974); R. A. Hulse and J. H. Taylor, *Astrophys. J.* **195**, L51 (1975).
2. J. P. Ostriker and J. E. Gunn, *Astrophys. J.* **157**, 1395 (1969).
3. J. M. Comella, H. D. Croft, R. V. E. Lovelace, J. M. Sutton, *Nature (Lond.)* **221**, 453 (1969).
4. M. I. Large, A. E. Vaughan, R. Wielebinski, *ibid.* **220**, 754 (1968).
5. W. J. Cocke, M. J. Disney, D. J. Taylor, *ibid.* **221**, 525 (1969).

6. G. J. Fishman, F. R. Harnden, R. C. Haymes, *Astrophys. J.* **156**, L107 (1969).
7. R. Giacconi, S. Murray, H. Gursky, E. Kellogg, E. Schreier, T. Matilsky, D. Koch, H. Tananbaum, *Astrophys. J. Suppl. Ser.* **27**, 37 (1974).
8. B. Margon and A. Davidsen, *Int. Astron. Union Circ. 2712* (24 Oct. 1974).
9. G. Baym, C. Pethick, P. Sutherland, *Astrophys. J.* **170**, 299 (1971).
10. Z. Kopal, *Close Binary Systems* (Wiley, New York, 1959).
11. C. W. Allen, *Astrophysical Quantities* (Athlone, London, 1963).
12. S. Van den Bergh, A. P. Marscher, Y. Terzian, *Astrophys. J. Suppl. Ser.* **26**, 19 (1973).
13. D. K. Milne, *Aust. J. Phys.* **23**, 425 (1970); D. Downes, *Astron. J.* **76**, 305 (1971).
14. R. Kippenhahn, K. Kohl, A. Weigert, *Z. Astrophys.* **69**, 265 (1968).
15. R. P. Kraft, *Astrophys. J.* **135**, 408 (1962); B. Warner and R. E. Nather, *Mon. Notic. R. Astron. Soc.* **152**, 219 (1971).
16. P. Giannone and A. Weigert, *Z. Astrophys.* **67**, 41 (1967).
17. W. K. Rose, *Astrophys. J.* **152**, 245 (1968).
18. S. Starrfield, W. M. Sparks, J. W. Truran, *ibid.* **192**, 647 (1974); *Astrophys. J. Suppl. Ser.* **28**, 247 (1974).
19. J. Faulkner, *Astrophys. J.* **170**, L99 (1971).
20. W. M. Sparks and T. P. Stecker, *ibid.* **188**, 149 (1974).
21. G. Shaviv and N. Vidal, *Astrophys. Space Sci.* **15**, 195 (1972); T. J. Mazurek, *ibid.* **23**, 365 (1973).
22. S. A. Colgate and R. H. White, *Astrophys. J.* **143**, 626 (1966).
23. This work was supported in part by the National Science Foundation under grant MPS 74-13257.

\* On leave from the Astronomy Department, University of South Florida, Tampa 33620.

29 November 1974; revised 14 March 1975

## Laser Raman Spectroscopy—New Probe of Myosin Substructure

**Abstract.** *Laser Raman spectroscopy is used to probe the heterogeneous substructure of the large contractile protein myosin. Some peaks are assigned to specific chemical groups of the molecule; others, notably the conformationally sensitive amide III vibrations, provide information on the structurally distinct regions of the molecule. Deuteriation of the NH groups is instrumental in the assignment of these vibrational modes. The relative intensities of bands typical of  $\alpha$ -helical conformations (near 1265 and 1304  $cm^{-1}$ ) and bands associated with nonhelical structure (near 1244  $cm^{-1}$ ) are sensitive indicators of myosin substructure and represent potentially useful probes of conformational changes.*

Myosin, one of the chief constituents of the contractile apparatus of muscle (and other motile systems), accounts for approximately half of myofibrillar protein. Myosin contains two  $\alpha$ -helical heavy chains ( $\sim 200,000$  daltons each) twisted around each other to form a long coil (Fig. 1a); each heavy chain terminates in a globular head portion (1, 2). Most of the long coil portion can be isolated by limited tryptic digestion of myosin (3, 4) as the light meromyosin. Each globular head portion is associated with two small peptide chains ( $\sim 20,000$  daltons each) and contains functionally important sites for interactions with actin and adenosine triphos-

phate (5). Such interactions associated with conformational changes (5, 6) of myosin are considered to play a crucial role in the molecular mechanism underlying muscle contraction.

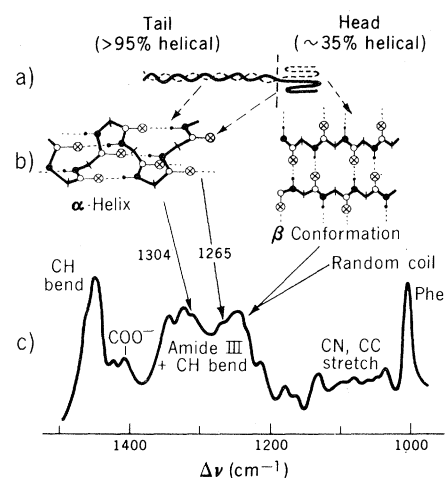


Fig. 1. One possible correlation of (a) the structurally distinct subregions of myosin, (b) their proposed conformational structures, and (c) the Raman spectrum of the amide III region of myosin. Arguments favoring this interpretation of the spectral results are presented in the text.